Incorporation of iodine into uranophane formed during the corrosion of spent nuclear fuel

By S. Wu[1,2], F. Chen[3,*], M. Kang[1,2], Y. Yang[1] and S. Dou[1,2]

[1] Guangzhou Institute of Geochemistry, Chinese Academy of Sciences, Guangzhou 510640, China
[2] Graduate University, Chinese Academy of Sciences, Beijing 100049, China
[3] Nanjing University, Nanjing 210093, China

Summary. In order to evaluate the potential incorporation of ^{129}I into uranyl phases that would form during oxidative alteration of spent nuclear fuel, uranophane was synthesized under mild hydothermal conditions of 165 °C in the presence of iodide, iodate and periodate, respectively. The precipitates were examined and analyzed using powder X-ray diffraction (XRD), infrared spectroscopy (IR) and scanning electron microscope (SEM) equipped with an energy-dispersive X-ray spectroscopy (EDS). The results indicate that significant amount iodine can be incorporated into the structure of uranophane in the form of IO_4^-, and less in the form of IO_3^-. Crystallo-chemical analyses suggest that the incorporation mechanisms would be the substitution of iodate and periodate for SiO_4 tetrahedron in the sheet.

1. Introduction

The safe disposal of high-level nuclear waste (HLW) has been a huge challenge worldwide. After four decades of study, geological disposal remains the only scientifically and technically credible long-term solution available to permanent isolation of the radionuclides from biosphere [1]. Up to 270 000 tons of spent nuclear fuel (SNF) had been accumulated in the world by 2007, and the global amount of SNF increases by 12 000 tons each year [2].

^{129}I is a long-lived isotope of iodine with a half-life of 1.6×10^7 years, and is generated in nuclear reactors as a fission product. The net production of ^{129}I from ^{235}U fission in a thermal reactor is about $1 \, \mu\text{Ci} \, \text{MW}^{-1} \, \text{d}^{-1}$, depending upon the neutron flux and irradiation time [3], resulting in as much as 0.2 kg of ^{129}I in each metric ton of spent nuclear fuel [4]. It was estimated that more than 54 000 kg of ^{129}I had been accumulated in SNF all over the world by 2007. In addition, more than 5068 kg of anthropogenic ^{129}I has been released into the global environment [5]. Because iodine is highly mobile in most geochemical environments, ^{129}I is considered to have a high potential of escaping into the biosphere.

Based on the performance assessment of the proposed repository at Yucca Moutain, USA [6, 7], it is clear that ^{129}I is one of the limited number of radionuclides that make the dominant contribution to final dose calculations. Therefore, the behavior and fate of ^{129}I released from altered nuclear waste is important in the safety analysis of nuclear waste repositories.

On the other hand, a large amount of uranyl phases are expected to form during the alteration of UO_2 matrix in SNF especially at the presence of radioactively produced oxidants [8–11], and the radionuclides released from the altered nuclear fuel may become incorporated into the secondary uranyl phases [12–15], resulting in near-field containment.

Uranophane is the most common uranium(VI) mineral in nature [16] and is expected to be one of the dominant alteration products of SNF in a geologic repository under oxidizing conditions [14, 17, 18]. The possible incorporation of iodine into the structure of uranophane may significantly reduce the mobility of the ^{129}I in geologic repositories.

2. Materials and methods

2.1 Synthesis of uranophane

Uranophane was synthesized with reagent grade or purified chemicals following the procedure of Oji [19] with some amelioration. An aqueous solution was made by mixing 5 ml 0.1 M uranyl acetate, 2.5 ml 0.2 M sodium silicate and 5 ml 0.1 M calcium nitrate at room temperature in a Teflon-lined Parr vessel under continuous stirring. The solution pH was adjusted to about 10 using 1 M NaOH. The solution was aged at room temperature for 2 d and then heated at 165 °C in an oven. After 7 d, the vessel was removed from the oven and cooled to room temperature. The suspension was filtered and the precipitate was rinsed with 18 MΩ de-ionized (DI) water to remove excess starting materials, then dried in air. A bright butter yellow powder was obtained.

In order to examine the possible incorporation of iodine into the synthesized crystals, ^{127}I was used as the surrogate of ^{129}I in the synthesis, and I^-, IO_3^- and IO_4^- were added initially as KI, KIO_3 and KIO_4, with I : U molar ratios of 1 : 1, 1 : 5 and 1 : 10, respectively. The details of the experiments are given in Table 1. In the presence of iodine,

---

Table 1. Details of the experiment.

Sample	Molar$_{I:U}$	pH		
		Before aged	After aged	After reaction
U	0	10.35	9.60	6.17
U-KIO$_3$-1 : 1	1 : 1	10.63	9.57	5.46
U-KIO$_3$-1 : 10	1 : 10	10.83	9.73	7.60
U-KIO$_4$-1 : 1	1 : 1	10.63	7.63	5.86
U-KIO$_4$-1 : 10	1 : 10	10.33	9.29	6.01
U-KI-1 : 1	1 : 1	10.81	9.68	7.66
U-KI-1 : 10	1 : 10	10.85	9.71	7.64

the powders were washed with ethanol, after washing with deionized water, to remove the molecule iodine (I$_2$) that would be produced during the synthesis.

2.2 Analytical methods

pH was measured with a PD-501 pH meter and Orion glass body combination pH probe. Solids were characterized using powder X-ray diffraction (XRD), infrared spectroscopy (IR), scanning electron microscope equipped with an energy-dispersive X-ray spectroscopy (SEM-EDS), thermal analysis (TA), and X-ray photoelectron spectroscopy (XPS).

Powder XRD analyses were obtained by using Rigaku D/max-IIIA diffractometer with Cu K_α radiation (30 mA and 40 kV), between 3° and 80° (2θ) at a step of 0.02° with a scanning speed of 8°/min. Identifications of solid phases were made by comparing the diffraction patterns to a database of ICDD-PDF reference patterns.

IR data were collected on a SP 2000 (Pye Unicam Ltd.) infrared spectrometer by using the KBr pressed disk technique. 32 scans were collected for each measurement over the spectral range of 400–4000 cm^{-1} with a nominal resolution of 4 cm^{-1}.

Samples to be analyzed by SEM/EDS were mounted on stainless steel stubs and gold-coated. A Quanta 400 (FEI company) scanning electron microscope equipped with a Genesis 2000 energy-dispersive X-ray spectroscopy (EDAX company) was operated at an accelerating voltage of 20 kV to examine the morphology and analyze the chemical variation of the synthsized crystals.

Thermal data for the synthetic phases were collected by using NETZSH STA 409 PC/PG. Samples (15–40 mg) were encapsulated in Al$_2$O$_3$ pans and heated at a rate of 10 K/min from 30 °C to 800 °C under a nitrogen atmosphere.

Solid surfaces were characterized by XPS at the "Instrumental Analysis & Research Center, Sun Yat-sen University" using a multidirectional electron energy analyzer (ESCALAB 250, Thermo-VG Scientific). Analyses were carried out by using a monochromatized Al K_α source (1486.6 eV) operated at 15 kV and 150 W. The analyzer chamber pressure was around 2×10^{-9} mbar. Survey spectra were recorded for each sample using a fixed pass energy of 70 eV, while high resolution spectra of Si 2p, Ca 2p, I 3d, U 4f, and O 1s levels were recorded using a pass energy of 20 eV. All high-resolution spectra were presented after a Shirley or a linear background subtraction.

3. Results and discussion

3.1 Mineral characterization

3.1.1 X-ray diffraction patterns

The SEM image shows that the uranophane appears as acicular or hair-like crystals that form radial aggregates and tufts (Fig. 1). The influence of iodine on the morphology of the crystals is not obvious.

The XRD pattern of the synthesized samples show peaks at 0.79 nm (*hkl*: 200), 0.395 nm (*hkl*: 400), 0.481 nm (*hkl*: 011), 0.298 nm (*hkl*: 012) and 0.32 nm (*hkl*: 220) (Fig. 2), which is in well agreement with that of uranophane (ICDD card #39-1360). No significant difference in XRD pattern is observed between the crystals that are produced with and without the presence of iodine, respectively. In addition, minor haiweeite (Ca(UO$_2$)$_2$Si$_6$O$_{15}$·5H$_2$O) [20] and weeksite (K$_2$(UO$_2$)$_2$Si$_6$O$_{15}$·4H$_2$O) [21] may have formed in the system with $n_{KIO_4} : n_{UO_2} = 1 : 1$ (Fig. 2) according to the XRD data.

3.1.2 Infrared spectroscopy

Infrared spectroscopy is widely used in analyzing the composition of natural and synthetic samples. This nondestructive method provides characteristic spectra that serve as fingerprints for the identification of minerals. IR data obtained for the samples of uranophane is listed in Table 2, and the literature data in Table 2 is given for comparison and identification [22, 23]. Although most of the bands of the synthesized uranophane in the presence of KI and KIO$_3$ fit very well to the references (Fig. 3), some band shifts are observed as KIO$_4$ content increases (Fig. 4), which suggest that IO$_4$ may be incorporated into the structure.

However, several shifts are observed when KIO$_4$ exist (Fig. 4). The band at 3427 cm^{-1} is attributed to the inner hydroxyl units. The band shifts to lower wavenumbers (3426 cm^{-1}, 3423 cm^{-1} and 3421 cm^{-1}) as the concentration of iodine increased. The band at 1634 cm^{-1} is assigned to water bending modes of the water in the hydration sphere within the uranophane interlayer. As the concentration of iodine increased, the band shifts to 1637 cm^{-1}, 1630 cm^{-1} and 1626 cm^{-1}, respectively. The infrared spectrum of SiO$_4^{4-}$ stretching bands show two strong absorptions at 1005 cm^{-1} and 940 cm^{-1} and two weak absorptions at 481 cm^{-1} and 455 cm^{-1}. As the concentration of iodine increased, the 1005 cm^{-1} band shifts to 1008 cm^{-1}, 1022 cm^{-1} and 1054 cm^{-1}, respectively. Furthermore, a new small weak band at 1018 cm^{-1} is observed when $n_{KIO_4} : n_{UO_2} = 1 : 1$. The 940 cm^{-1} band shifts to 939 cm^{-1}, 932 cm^{-1}, 913 cm^{-1} and 445 cm^{-1} band shifts to 446 cm^{-1}, 451 cm^{-1}, 453 cm^{-1}. The 481 cm^{-1} band shifts to 479 cm^{-1}, 477 cm^{-1} and then lost when $n_{KIO_4} : n_{UO_2} = 1 : 1$. The bands at 855 cm^{-1} and 660 cm^{-1} are attributed to UO$_2^{2+}$ unit. These band shifts to higher wavenumbers as the concentration of iodine increased, 855 cm^{-1} to 855 cm^{-1}, 859 cm^{-1} and 866 cm^{-1}, 660 cm^{-1} to 661 cm^{-1}, 662 cm^{-1} and 682 cm^{-1}. Additionally, the intensity in 1041 cm^{-1} band is stronger while iodine existence. These shifts indicated that periodate has been incorporated into the crystal of uranophane.

Čejka [22] suggested that the weak bands observed in the range 1200–1550 cm^{-1} may be assigned to δ SiOH. How-
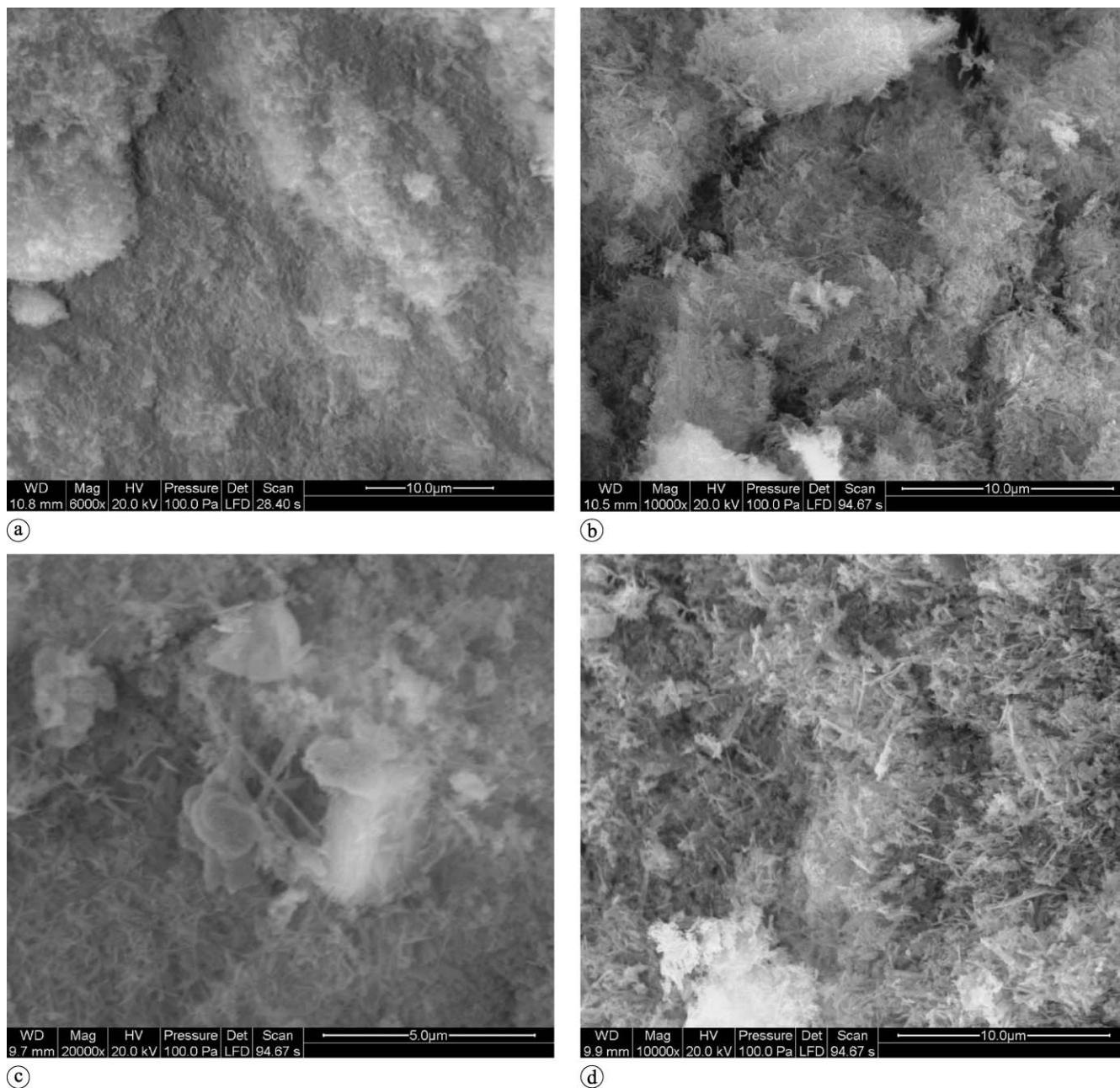
Fig. 1. SEM micrograph of uranophane crystals from 7 d tests (**a**, U; **b**, U-KIO$_3$-1 : 1; **c**, U-KIO$_4$-1 : 1; **d**, U-KI-1 : 1).

Table 2. IR band maxima of uranophane, and the tentative assignment of the bands.

Uranophane (Čejka [22]; Lehmann *et al.* [23])	Uranophane (this study)	U-KIO$_3$-1 : 10	U-KIO$_4$-1 : 10	U-KI-1 : 10	Tentative assignment
3437	3427	3427	3425	3426	ν OH
1632/1636	1633	1633	1636	1634	δ H$_2$O
1200–1550 w^a	1384	1384	1384	1384	ν_3 NO$_3^-$
	1143	1143	1147	1144	
1018	1004	1003	1008	1005	ν_3 SiO$_4^{4-}$
936	940	939	939	939	
855/859	854	856	857	857	ν_3 UO$_2^{2+}$
767/790	767	769	769	770	ν_1 UO$_2^{2+}$
564	559	558	560	559	ν_4 SiO$_4^{4-}$
480	481	481	479	482	ν_2 SiO$_4^{4-}$

a: w – weak.

ever, Lehmann *et al.* [23] found a sharp peak with high intensity at 1384 cm^{-1} and thought this spectral region is the ν_3 stretching mode of NO$_3^-$. Because Ca(NO$_3$)$_2$ was used as a initial material and the nitrate was detected by EDS in this study, we assign this band mainly to the ν_3 stretching mode of NO$_3^-$ as Lehmann *et al.* [23] suggested.
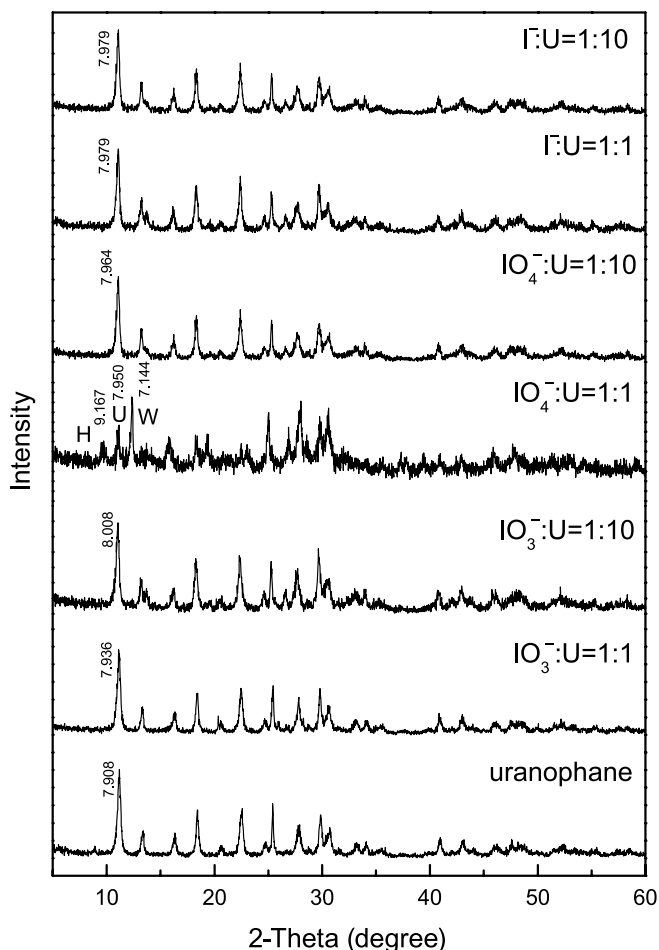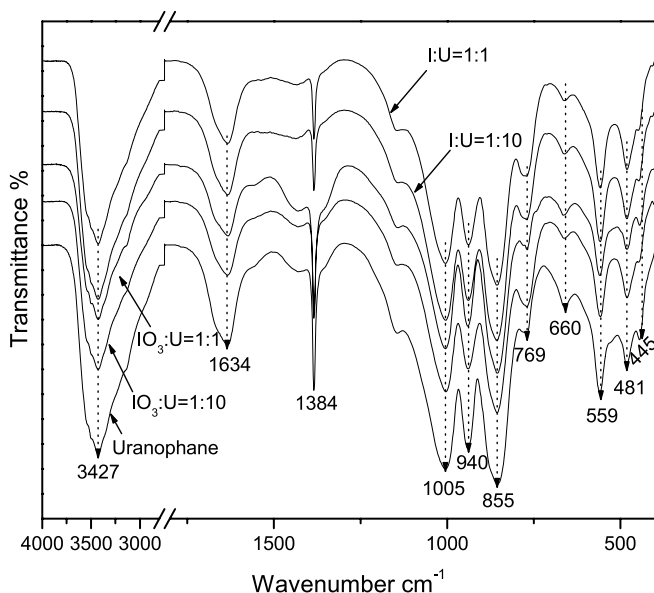
Fig. 2. XRD patterns of synthetic uranophane.

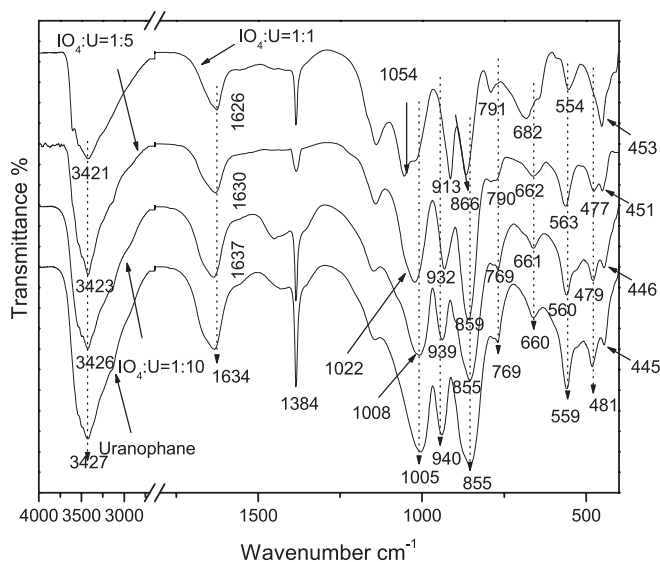**Fig. 3.** IR spectroscopy of uranophane (U-KI, U-KIO$_3$).

Fig. 4. IR spectroscopy of uranophane (U-KIO$_4$).

(strong) with 2 H$_2$O dehydration, and other dehydration inflexions were at 155–480 °C (1 H$_2$O) and 480–820 °C (1.5 H$_2$O). In most cases, the last two inflexions were not observed clearly based on the DTG curve, while the samples with endotherms at 155–480 and 480–820 °C show endotherms at different temperatures. For example, the DTG curve of sample U-KI-1 : 1 that is synthesized in the presence of iodide has endotherms at 335.4 and 709.6 °C; the curve of sample U-KIO$_3$-1 : 1 shows endotherms at 111.9, 169.7, 267.6, 338.7 and 586.7 °C, while U-KIO$_4$-1 : 10 at 106.3, 162.5 and 718.9 °C. These observations confirm that high purity uranophane was synthesized in the experiments, and suggest that the existence of iodate and periodate may impact the thermal behavior of uranophane.

3.2 Iodine content in the sythesized uranophane

Energy dispersive X-ray spectroscopy was used to analyze the samples in order to know whether iodine can be incorporated into the crystals. Because the crystal was washed with de-ionized water for 5 times, followed by washing with ethanol, the iodine detected is considered to be incorporated into the structure of the crystals.

Table 3 shows the concentration of incorporated iodine in some synthetic samples, while others without iodine were not shown here. According to the EDS results, both iodate and periodate were found in uranophane. As the molar ratio

3.1.3 Thermal behavior

The DTG curve of synthetic crystals is in general agreement with that of uranophane reported by Čejka [22] (Fig. 5). According to Čejka [22], the endotherm at 96.9 °C (weak) was associated with 1 H$_2$O dehydration, 148.1 °C

Table 3. Concentration of incorporated iodine in synthetic uranophane.

Sample	Average concentration of iodine (%)	Average concentration of uranium (%)	I : U (%)
U-KIO$_3$-1 : 1	0.21	43.02	0.49
U-KIO$_4$-1 : 10	0.25	41.56	0.60
U-KIO$_4$-1 : 5	0.66	40.52	1.63
U-KIO$_4$-1 : 1	5.17	40.20	12.86

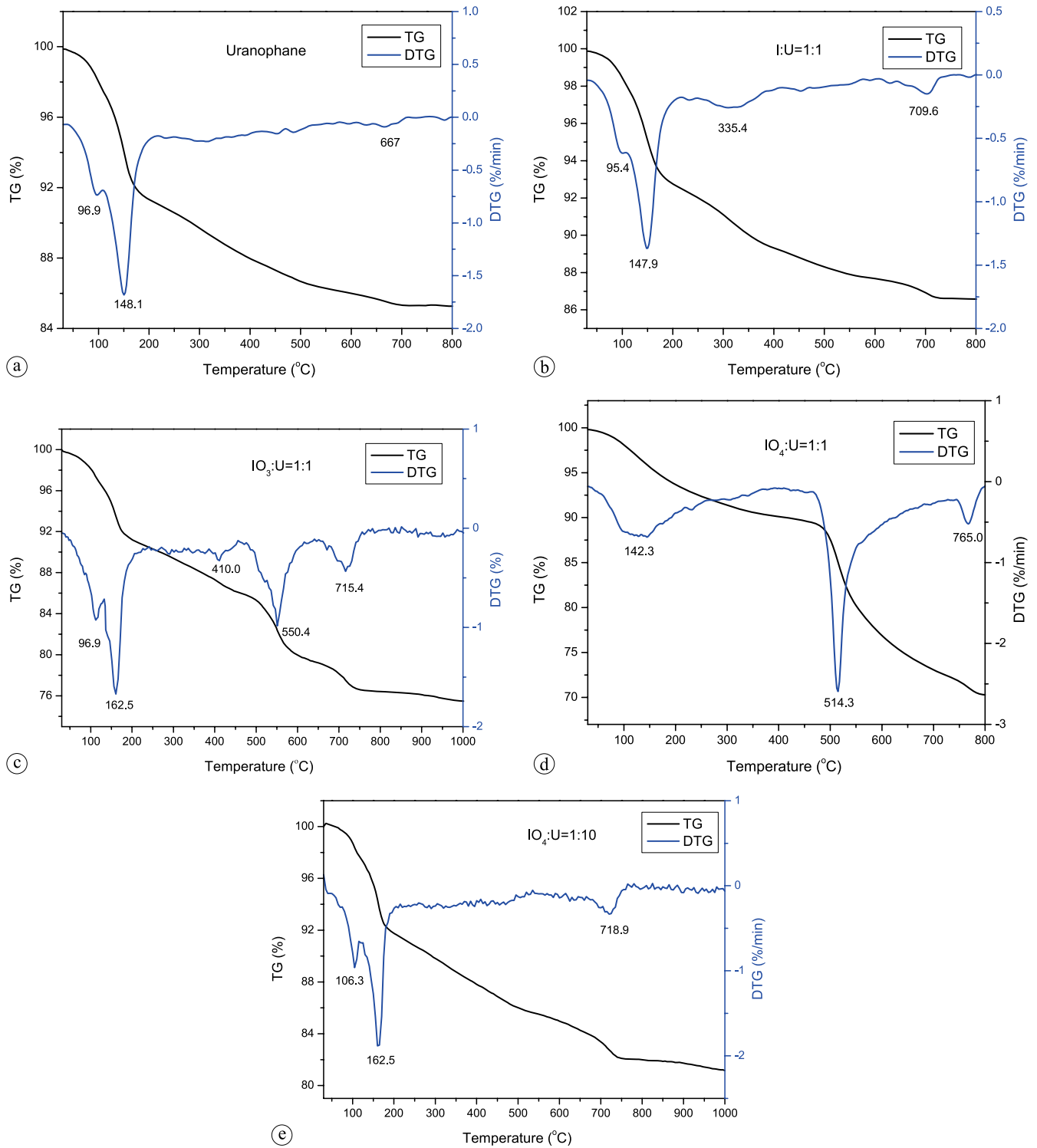**Fig. 5.** TG and DTG of synthetic uranophane.

of IO_4^- : U increases from 1 : 10 to 1 : 1 in the initial solutions, the iodine content in the uranophane crystals increases from 0.60% to 12.86%. In cases of the presence of iodate, iodine was detected only in the samples that are produced in solution of IO_3^- : U = 1 : 1. However, the iodine content in samples that are produced in the presence of iodide is under the detection limit of EDS. These observations suggest that a significant amount of iodine could be incorporated into uranophane in the form of IO_4^-, and less in the form of IO_3^-, while little I^- would be absorbed into the structure.

3.3 Incorporation mechanism of iodine into uranophane

Because iodine is a redox sensitive element, XPS was used to identify the valence of the iodine that is incorporated into the synthesized uranophane (Fig. 6). The results showed that C, O, Si, Ca, U and I were observed in the samples that were synthesized in KIO_4 bearing solutions. The binding energy of I $3d_{5/2}$ in the uranophane is 623.8 eV, which is in agreement with the value of potassium periodate (624 eV)
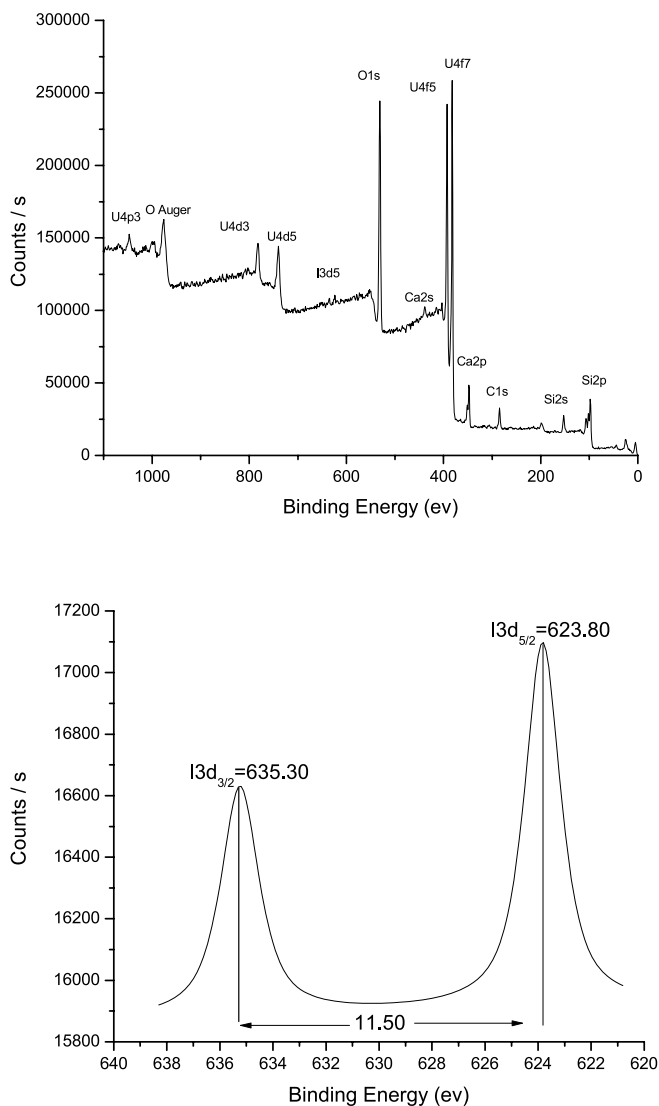
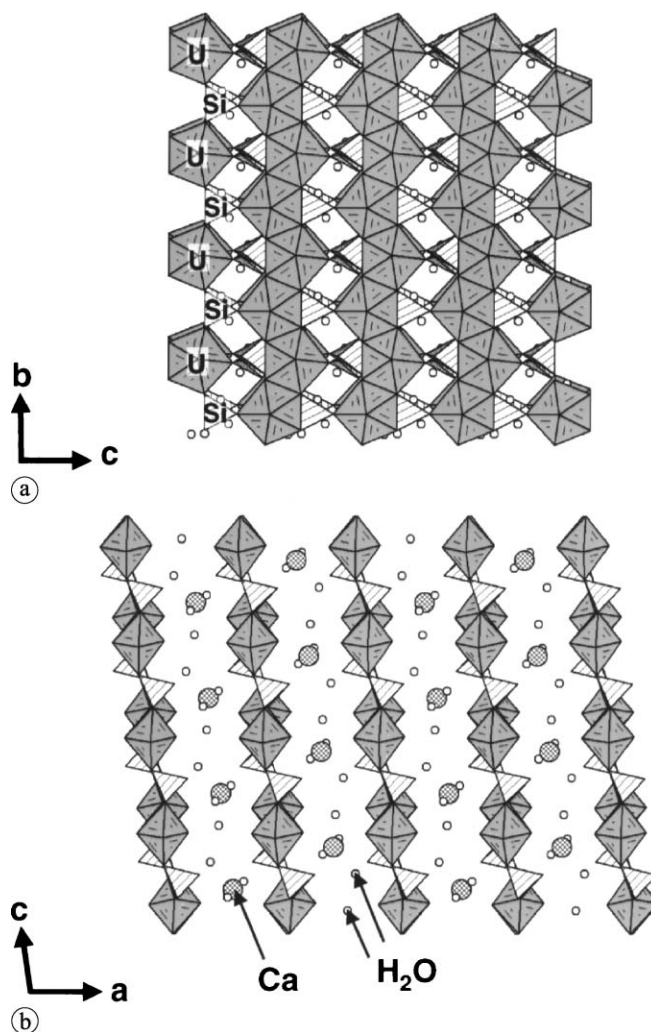**Fig. 6.** XPS survey of U-KIO$_4$-1 : 10 and the I $3d$ scan.

Fig. 7. The structure of uranophane viewed along (**a**) [100] and (**b**) [010]. Ca and H$_2$O exist in the interlayer of the sheet structure. From Utsunomiya *et al.* [25] and after Burns [26].

from the National Institute of Standards and Technology XPS database, and is quite different from the values for iodate (623.3 to 623.5 eV) and iodide (618.4 to 618.5 eV) [24]. Thus, the binding energy of 623.8 eV for I $3d_{5/2}$ in uranophane may be attributed to periodate, and the 0.2 eV shift should be caused by the difference in chemical environment around iodine. This observation indicates that the valent state of iodine did not change during the mineral synthesis.

As shown in Fig. 7, uranophane consists of alternating stacks of U−Si−O sheets with interlayer cations bonded to water molecules or hydroxyl in the α-direction [25]. The sheet contains chains of edge-sharing UO$_5$ polyhedra that are cross-linked *via* SiO$_4$ tetrahedra [13] by sharing two oxygen atoms. In SiO$_4$ tetrahedra, the Si−O bond distances are from 1.560 Å to 1.700 Å with an average value of 1.624 Å [21, 27, 28]. Most uranyl iodates contain UO$_6$ hexagonal bipyramids and/or UO$_5$ pentagonal bipyramids, and iodate/periodate ligands are connected to the bipyramids by sharing oxygen atoms. In these compounds I−O bond distances of IO$_3$ are from 1.772 Å to 1.858 Å, and the average value is 1.809 Å [29–32]. IO$_4$ structure is observed in one compound, Ag$_4$(UO$_2$)$_4$(IO$_3$)$_2$(IO$_4$)$_2$O$_2$, in which the average I−O bond distance is 1.909 Å and IO$_4$ sharing

two oxygen with UO$_5$ polyhedra [29]. The similar role of iodate/periodate and SiO$_4$ tetrahedra in the uranyl crystals imply that the substitution of iodate/periodate for SiO$_4$ is possible.

According to the XRD patterns of uranophane which was synthesized in the presence of iodine, the crystal structure is in excellent agreement with natural uranophane, indicating that with the incorporation of iodine into the crystal, the structure kept stable. Thus, the substitution for SiO$_4$ tetrahedron should be used to explain the role of iodine in the crystals. The ionic radius of I^{7+} is 0.053 nm, which is more similar with Si^{4+} (0.040 nm) than I^{5+} (0.095 nm) [33]. It may be the reason that periodate can be incorporated into uranophane easier than iodate, thus the ionic radius is determinant in this case. Moreover, both SiO$_4$ and IO$_4$ have a structure of tetrahedron in uranophane, and the substitution IO$_4 \leftrightarrow$ SiO$_4$ is more likely to occur. However, IO$_3{}^-$ usually has triangle coordination geometry with the three oxygen anions approximately in the plane of the sheet. Therefore, when IO$_3$ substitute for SiO$_4$, an angle of the SiO$_4$ will miss and more intensive structure adjustment is needed. Considering the charge balance, two hydroxyl groups should be linked to IO$_4$ or IO$_3$OH through hydrogen bond. Therefore, (IO$_4{}^-$)(OH$^-$)$_2 \leftrightarrow$ (SiO$_3$OH)$^{3-}$ and (IO$_3{}^-$)(OH$^-$)$_2 \leftrightarrow$

$(SiO_3OH)^{3-}$ should be possible. With the incorporation of iodine into the crystal, the vibrational spectra of SiO_4 shifts from 1005 to 1008, 1022 and 1054 cm^{-1}, respectively, this is considered to result from the substitution of SiO_4 by IO_4.

Nevertheless, iodide was not detected in this study. There are two reasons to explain the results. One is that iodide can not be incorporated into the uranophane crystal because of its large ionic radius (0.220 nm [33]), and the other one is that the content of incorporated iodide is lower than the detection limit of EDS.

4. Conclusions

The potential for ^{129}I incorporation into uranophane has been evaluated by precipitating uranophane from aqueous solutions containing KI, KIO$_3$ or KIO$_4$, and pure uranophane was obtained in the experiments. XRD patterns and IR spectrum indicated that with the incorporation of iodine into uranophane, the structure of the crystals kept stable. According to EDS results, both iodate and periodate were found in uranophane, and IO_4^- can be incorporated into uranophane easier than IO_3^-. It was suggested that the incorporation mechanisms for iodate and periodate in uranophane should be the substitution for SiO_4 in the sheet.

References

1. Committee on Disposition of High-Level Radioactive Waste Through Geological Isolation, Board on Radioactive Waste Management, National Research Council: *Disposition of High-Level Waste and Spent Nuclear Fuel: The Continuing Societal and Technical Challenges*. National Academy Press, Washington, DC (2001).
2. WNA (World Nuclear Association): www.world-nuclear.org/info/inf04.html (2007).
3. NCRP (National Council on Radiation Protection and Measurements): *Iodine-129, Evaluation of Release from Nuclear Power Generation* (1983).
4. Mtingwa, S. K.: In: An International Spent Nuclear Fuel Storage Facility-Exploring a Russian Site as a Prototype: Proceedings of an International Workshop. (Schweitzer, G. E., Sharber, A. C., eds.) The National Academies Press, Washington, DC (2005), p. 30.
5. Aldahan, A., Alfimov, V., Possnert, G.: Appl. Geochem. **22**, 606 (2007).
6. CRWMS M&O (Civilian Radioactive Waste Management System, Management and Operating Contractor): Total System Performance Assessment – 1995: An Evaluation of the Potential Yucca Mountain Repository, B00000000-01717-2200-00136,
Rev. 01, TRW Environmental Safety Systems, Inc., Las Vegas, NV (1995).
7. Kessler, J. H.: Electric Power Research Institute prepared by Quanti Sci. Inc., Vol. TR – 107190 3294-18 (1996).
8. Forsyth, R. S., Werme, L. O.: J. Nucl. Mater. **190**, 3 (1992).
9. Wronkiewicz, D. J., Bates, J. K., Gerding, T. J., Veleckis, E., Tani, B. S.: J. Nucl. Mater. **190**, 107 (1992).
10. Wronkiewicz, D. J., Bates, J. K., Wolf, S. F., Buck, E. C.: J. Nucl. Mater. **238**, 78 (1996).
11. Wronkiewicz, D. J., BucK, E. C.: In: *Uranium: Mineralogy, Geochemistry and the Environment*. (Burns, P. C., Finch, R. J., eds.) Mineralogical Society of America, Washington, DC (1999), p. 475.
12. Finn, P. A., Hoh, J. C., Wolf, S. F., Slater, S. A., Bates, J. K.: Radiochim. Acta **74**, 65 (1996).
13. Burns, P. C., Ewing, R. C., Miller, M. L.: J. Nucl. Mater. **245**, 1 (1997).
14. Buck, E. C., Finch, R. J., Finn, P. A., Bates, J. K.: Mater. Res. Soc. Symp. Proc. **506**, 87 (1998).
15. Chen, F. R., Burns, P. C., Ewing, R. C.: J. Nucl. Mater. **275**, 81 (1999).
16. Smith, D. K.: In *Uranium Geochmistry, Mineralogy, Geology, Exploration and Resources*. (DeVivo, B., Ippolito, F., Capaldi, G., Simpson, P. R., eds.) Institute of Mining and Metallurgy, London (1984), p. 43.
17. Finch, R. J., Murakami, T.: In *Uranium: Mineralogy, Geochemistry and the Environment*. (Burns, P. C., Finch, R. J., eds.) Mineralogical Society of America, Washington, DC (1999), Vol. 38, p. 91.
18. Long, L., Fanrong, C., Ewing, R. C.: Radiochim. Acta **95**, 25 (2007).
19. Oji, L. N.: Aiken, SC 29808 (2004), Vol. WSRC-TR-2003-00553.
20. Burns, P. C.: Can. Mineral. **39**, 1153 (2001).
21. Stohl, F. V., Smith, D. K.: Am. Mineral. **66**, 610 (1981).
22. Čejka, J.: In *Uranium: Mineralogy, Geochemistry and the Environment*. (Burns, P. C., Finch, R., eds.) The Mineralogical Society of America, Washington, DC (1999), Vol. 38, p. 521.
23. Lehmann, S., Geipel, G., Foerstendorf, H., Bernhard, G.: J. Radioanal. Nucl. Chem. **275**, 633 (2008).
24. NIST (National Institute of Standards and Technology): http://srdata.nist.gov/xps/.
25. Utsunomiya, S., Wang, L., Douglas, M., Clark, S. B., Ewing, R. C.: Am. Mineral. **88**, 159 (2003).
26. Burns, P. C.: In: *Uranium: Mineralogy, Geochemistry and the Environment*. (Burns, P. C., Finch, R., eds.) The Mineralogical Society of America, Washington, DC (1999), Vol. 38, p. 23.
27. Smith, D. K., Gruner, J. W., Lipscomb, W. N.: Am. Mineral. **42**, 594 (1957).
28. Barinova, A. V., Rastsvetaeva, R. K., Sidorenko, G. A., Pushcharovskii, D. Y.: Dokl. Chem. **378**, 122 (2001).
29. Bean, A. C., Campana, C. F., Kwon, O., Albrecht-Schmitt, T. E.: J. Am. Chem. Soc. **123**, 8806 (2001).
30. Sykora, R. E., Bean, A. C., Scott, B. L., Runde, W., Albrecht-Schmitt, T. E.: J. Solid State Chem. **177**, 725 (2004).
31. Bean, A. C., Ruf, M., Albrecht-Schmitt, T. E.: Inorg. Chem. **40**, 3959 (2001).
32. Ling, J., Albrecht-Schmitt, T. E.: Inorg. Chem. **46**, 346 (2007).
33. Shannon., R. D. (ed.): *Revised Effective Ionic Radii and Systematic Studies of Interatomic Distances in Halides and Chalcogenides*. Central Research and Development Department, Experimental Station, E. I. Du Pont de Nemours and Company, Wilmington (1976), Vol. A32.